

Leaky Mode Analysis of Solid Dielectric Horn Antenna

Shreya S. Menon^{1,*}, Shubham Kalra², Surya K. Pathak³, Nalesh Sivanandan¹, and Supriya M. Hariharan¹

¹Department of Electronics, Cochin University of Science and Technology, Cochin 682022, India

²Antsys Innovations Pvt. Ltd., Rajasthan, India

³HBNI, Institute for Plasma Research, Gandhinagar, India

ABSTRACT: Solid dielectric horn antennas have a directional radiation pattern and high gain. However, even when a solid dielectric horn antenna is excited with the fundamental mode metallic waveguide, there is a possibility that higher order modes in the guided region will be generated. Also, the energy can leak from the normal direction to the dielectric horn generating a leaky mode. It is one of the reasons that higher-order guided modes and leaky modes analysis of horn becomes important. In this paper, propagation characteristics for solid dielectric horns are derived and computed for fundamental and higher-order guided and also leaky modes in a solid dielectric horn antenna. We have also analyzed the radiation characteristics of the leaky mode and guided mode of a solid dielectric horn. Finally, radiation equations for a solid dielectric horn antenna that were deduced earlier by some of the authors, but omitted for brevity are given and compared with numerical and measured results. These results have been further verified by comparing them with the already reported literature on guided mode radiation characteristics of the solid dielectric horn. From the plotted graphs given in the paper, we can infer that the proposed propagation constant equations and radiation equations predict dispersion characteristics and the radiation pattern of guided and leaky modes well, respectively.

1. INTRODUCTION

Dielectric antennas employ a system of dielectric elements to radiate or receive electromagnetic energy, unlike dielectric lens antennas, which are secondary radiators used for phase corrections. These primary antennas can be of many shapes like cones, cylinders, spheres, rectangular rods, circular and rectangular horns, or any other shape [1]. Dielectric antennas generally have directional radiation patterns. They can be lightweight and have non-corrosive properties. Therefore, they can be used in applications where plasma can interact with metals like plasma diagnostics to enhance the radiation characteristics of microwave reflector antennas, thereby reducing spillover and providing more uniform reflector illumination [2]; as loads for metallic horns to modify the radiation pattern; as an embedded antenna in integrated circuits receiver [3]; in millimeter wave [4–8]; and as phased array elements [7–10]. Tapered rods, with their large and efficient launching aperture, and solid dielectric horns, with their large radiating aperture, have been popular for some time [11, 12]. A solid dielectric horn antenna is preferred over a tapered rod antenna, which has more radiation leaks, and the leaks do not contribute usefully to the radiation pattern. In dielectric horn antenna, the throat end prefers E plane field taper [13] over the other types and is tightly fitted into a metallic waveguide feed as shown conceptually in Fig. 1. When a solid dielectric horn antenna is excited with the fundamental mode metallic waveguide, there is a possibility that higher order modes in the guided region will be generated. Also, the energy can leak from the normal direction to the dielectric horn, generating a leaky mode. Further, solid dielectric horn antenna can work in leaky mode region by using

a few strips on sides [14]. They are some of the reasons that leaky mode analysis of horn becomes important. Some authors have modeled a solid dielectric horn antenna, including a transition for eliminating higher-order modes in solid dielectric horns with high dielectric constant material [15]. This transition has been fabricated. There has been very little documented literature on the comparison of analytical and simulated modal characteristics of the higher-order guided modes or the propagation and radiation characteristics of leaky modes in a solid dielectric horn antenna. In this paper, we propose a detailed theory for propagation characteristics for fundamental and higher order TE to x mode and the theory for radiation of leaky modes in a solid dielectric horn antenna (omitted earlier for brevity) and also successfully verify them with simulated and measured results.

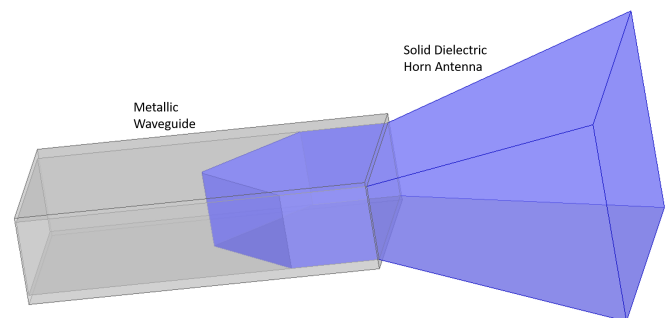


FIGURE 1. Solid dielectric horn antenna with E -plane taper and $\epsilon_r = 3.4$.

* Corresponding authors: Shreya S. Menon (shreyasmenon@cusat.ac.in).

2. RELATED WORK

Far-field patterns of a dielectric horn antenna for various dielectric constants ($\epsilon_{r1} = 2.54, 2.56 \& 2.80$) at 9.42 GHz and their aperture/near field distribution are studied theoretically and experimentally in [16, 17]. The approximate surface fields are theoretically presented for the H plane sectoral dielectric horn antenna in [18]. An analysis of the aperture field of an E -plane sectoral solid dielectric horn antenna is described for the TE to x mode in [19]. The radiation characteristics of guided modes in a solid dielectric horn antenna are explored in [20]. The radiation patterns of pyramidal dielectric waveguides excited by pyramidal metallic horns are deduced and experimentally verified at 9 GHz in [21] for guided modes but not leaky modes. The radiation pattern of guided mode but not leaky modes in an E -plane sectoral solid dielectric horn antenna has been obtained in [22]. Near-field distributions of dielectric horn antennas are studied theoretically and experimentally in [23] for the dominant guided mode but not leaky mode mode. Theoretical analysis of propagation characteristics for higher-order guided modes is deduced in [24] for TM to y mode. Wang et al. [14] added tapered strip on the sides of the solid dielectric horn for generating leaky waves, thus reducing return loss. In [25], Roy et al. have worked on reducing the S_{11} of a metallic waveguide fed solid dielectric horn by using double-sided tapering at the horn throat.

However, until recently, as far as the authors' knowledge, there has not been literature on the comparison of analytical and simulated modal characterization of the higher-order guided modes or leaky modes and radiation characteristics of leaky modes in a solid dielectric horn antenna as proposed earlier by the authors in [15, 26]. These aspects are looked into in detail in this paper. The radiated E -field equations for a solid dielectric pyramidal horn, omitted earlier for brevity by some of the authors, are proposed for guided & leaky modes, and the results are compared with simulated and measured results. A solid dielectric horn antenna has been fabricated in perspex with a dielectric constant of 2.54, and its measurement results have been compared with the proposed theory and simulation results. Usually, the solid dielectric horn antenna is simulated or measured, but it does not point at the exact sources of the pattern in case higher-order modes or leaky modes are also getting excited. The theory of radiation proposed in this paper will help us deduce the sources of the pattern. It is hence a platform for further theoretical analysis (e.g.; array environment, parametric sweeps).

The organization of the paper is as follows. Section 3 presents the theory involved in the propagation characteristics of a solid dielectric horn antenna. Section 4 presents radiation equations, as well as its comparison with simulated results. Section 5 presents measurement results, and the paper is concluded in Section 6.

3. PROPAGATION CHARACTERISTICS

The theoretical formulation for a solid dielectric horn antenna is similar to [15, 24] and is encapsulated as a flowchart in Fig. 2. The boundary conditions and field variations in each region have been described well in [27]. The solid dielectric horn is

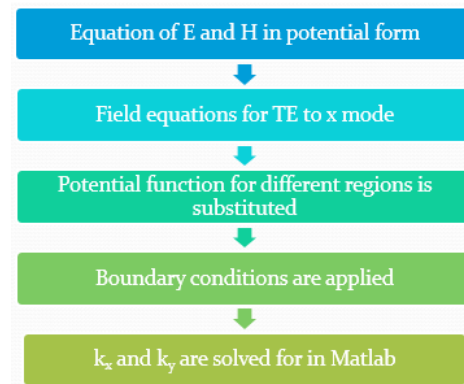


FIGURE 2. Flow chart revealing procedure adopted to find modal characteristics of solid dielectric horn antenna for TE to x mode.

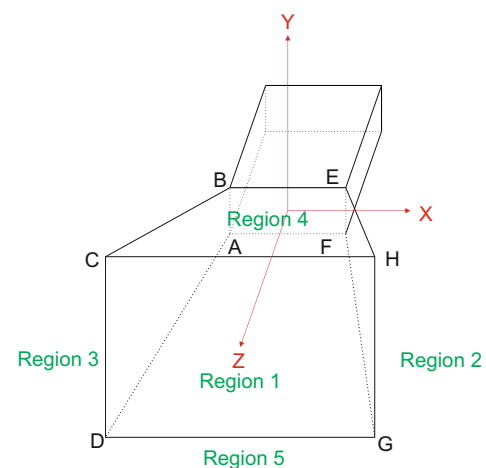


FIGURE 3. Various regions of the solid dielectric horn antenna.

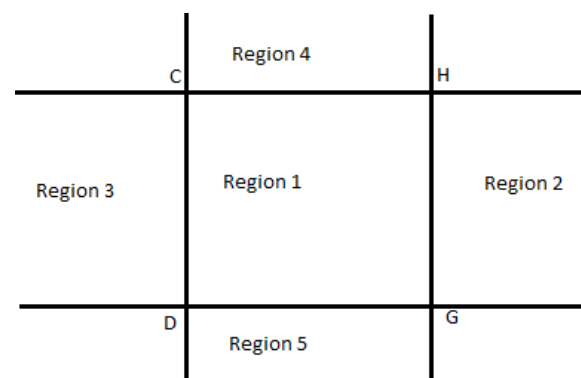


FIGURE 4. Front view of horn showing various regions of the solid dielectric horn antenna.

shown in Fig. 3 and Fig. 4 (where Region 1 is the region inside surfaces ABCD, FEHG, AFGD, and BEHC; Region 2 is the region in free space and to the right of Region 1, and so on) similar to [23, 24]. When the mode is guided, the transverse propagation constants, k_x and k_y in Regions 1, 2, 3, and 4, are real. However, forward leaky modes are complex depending on which side they leak from and explained in [28, 29]. They are also characterized by a negative imaginary part. Usually, it is desired for the antenna to work in the guided mode region as

the leaky mode region distorts the radiation pattern by leaking from the sides. Even though an analysis for the leaky mode region has been presented here in theory, the proposed antenna works in the guided mode region in the C-band, which is desirable for its radiation pattern purity. The analysis for leaky mode region is included here to give more clarity to designers on how they can be avoided and what type of pattern it can give rise to if somehow the leaky mode region happens to be unavoidable. Following the steps shown in Fig. 2, which uses the Marcatili's method [30], we have a set of equations for higher order guided and leaky modes [15], well explained in [27].

$$k_x \left(\frac{a}{2} + L \cdot \tan \alpha \right) = (m - 1)\pi + \tan^{-1} \left(\frac{\sqrt{k_1^2 - k_0^2 - k_x^2}}{k_x} \right) \quad (1)$$

$$k_y \left(\frac{b}{2} + L \cdot \tan \xi \right) = (n - 1)\pi + \tan^{-1} \left(\frac{\sqrt{k_1^2 - k_0^2 - k_y^2}}{k_y} \right) \quad (2)$$

where $m = 1, 2, 3 \dots$ & $n = 1, 2, 3 \dots$ are the order of modes; L is the axial length; α & ξ are the semi-flare angles along X -axis & Y -axis, respectively; a & b are the dimensions of the waveguide along X -axis & Y -axis, respectively. These are a set of transcendental equations that have to be solved iteratively for roots.

From the roots of these equations for transverse propagation constants, the axial propagation constant is found as

$$\beta_z = \sqrt{k_1^2 - k_x^2 - k_y^2} \quad (3)$$

This mode is TE to x mode, also known as the LSE_x mode (Longitudinal Section Electric) or the H^x mode.

For the modes that are guided, the propagation constant is given by [31]

$$k_0 < \beta_z < k_1 \quad (4)$$

or

$$1 < \beta_0 < \frac{k_1}{k_0} \quad (5)$$

where β_0 is the normalized axial propagation constant. When the modes are not guided in the structure, they leak from the sides and are called leaky modes. Unlike the guided modes, in such cases, β_0 is below 1. The plot of axial propagation constant against frequency is called the dispersion characteristics of a structure.

Higher values of dielectric constant lead to energy being more confined to the core, but the return loss characteristics are poor. For lower dielectric constant values, the return loss improves, but the possibility of leaky waves arises. Here, increasing the flare angle can lead to the waves being guided, but then the gain variation over the bandwidth is not linear (as expected for normal horn antennas with large flare angles), and the variation of the gain slope is large. One possible solution is to pick a low dielectric constant value and design the horn for a slightly lower cut-off frequency since, with frequency, the value of β_0 increases, and it can lead to the wave being guided at the desired frequency.

The solid dielectric horn antenna at its transition region from waveguide to the horn is a dielectric waveguide, so the same techniques that are used to excite a dielectric waveguide can be applied here. This excitation has two main aspects — exciting the metallic waveguide and employing a proper dielectric waveguide to metallic waveguide transition. The former is popularly done by exciting a probe inserted at the center of the broad side of the waveguide and at usually $\lambda/4$ distance from the shorted end (metallic wall) of the waveguide to excite the dominant TE₁₀ mode with proper matching [32]. A dielectric waveguide to metallic waveguide transition can be of different types like symmetric and asymmetric kinds of E -plane, H -plane, and pyramidal taper [13]. Of them, the symmetric kind of E -plane taper is an optimal transition for reasons mentioned in [13].

Plexiglass with a dielectric constant of 3.4 is used for leaky mode analysis. Tables 1 and 2 use (1) and (2) for tabulation. In Table 1, it is observed that the range of frequencies categorized as Leaky Antenna mode is widened further as ϵ_r is lowered and shifted to lower frequencies as the axial length is increased (keeping the flare angles same) as shown in Tables 1 and 2, respectively. The lower the value of the axial propagation constant is, the less guided it will be.

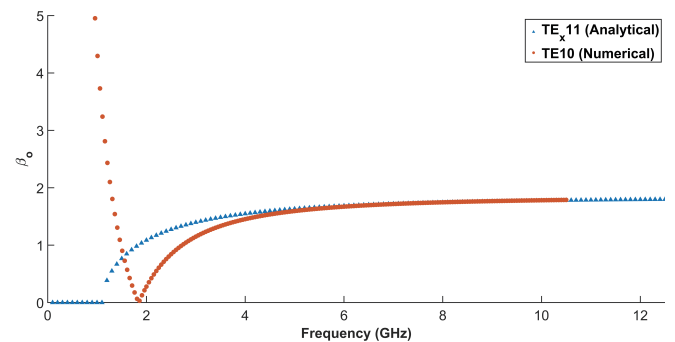


FIGURE 5. Normalized phase constant for TE_{x11} mode and $\epsilon_r = 3.4$.

The normalized propagation constant over frequency is analytically calculated and plotted for the proposed solid dielectric horn antenna with a dielectric constant of 3.4 and is compared with the simulated values. The results plotted in Fig. 5 of fundamental guided mode region and leaky mode region show a good agreement between them in the guided region ($\beta_0 > 1$) and not leaky mode region as the Marcatili method [30] is used where radiation from corners are ignored (see Fig. 4). This part is clearer in Table 3 and Fig. 6. The real part of the normalized axial propagation constant, β_0 , is below 1 for frequencies less than 1.9 GHz indicating leaky modes. Table 3 classifies the complete dispersion curve (Fig. 5) into 4 regions [33]. In the leaky reactive mode region, the normalized phase constant is less than 1 and less than the normalized attenuation constant, whereas, in the leaky antenna mode region, the normalized phase constant is less than 1 and greater than the normalized attenuation constant [33]. Table 3 shows the reactive mode region in simulated results as 'Non-available' because the simulated results do not show this region.

Figure 7 shows higher order modes generated with the help of (1) and (2). Fig. 8 shows the fundamental mode generated using

TABLE 1. Leaky antenna mode region for varying ϵ_r .

ϵ_r	2.4	3.4	4.3	10	11.9
Frequency range	0.9 to 2.3 GHz	1.2 to 1.8 GHz	1.1 to 1.5 GHz	0.9 GHz	0.8 GHz

TABLE 2. Leaky antenna mode region for varying axial length.

Axial length	20 mm	30 mm	40 mm	50 mm	60 mm
Frequency range	1.6 to 2.5 GHz	1.3 to 2.1 GHz	1.2 to 1.8 GHz	0.9 GHz	1.4 GHz

TABLE 3. Various regions for $\epsilon_r = 3.4$ and axial length = 40 mm.

Region	Analytical Result	Simulated result
Non-physical Leaky Mode	< 0.1 GHz	0.01 to 1.46 GHz
Leaky Reactive Mode	0.1 to 1.1 GHz	Non-available
Leaky Antenna Mode	1.2 to 1.8 GHz	1.51 to 2.7 GHz
Guided Mode	1.9 GHz & above	2.75 GHz & above

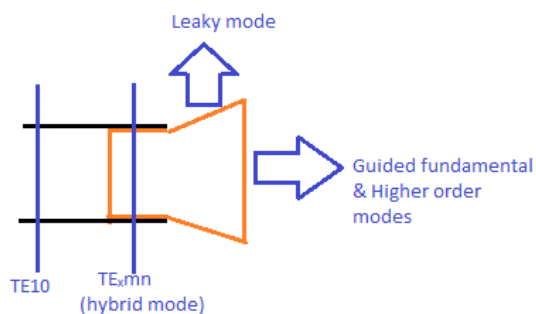


FIGURE 6. Working principle of different modes.

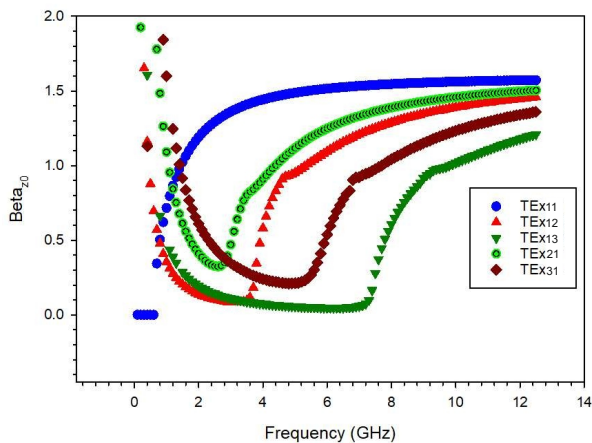


FIGURE 7. Normalized axial propagation plot of fundamental and higher order modes with $\epsilon_r = 2.54$.

theoretical and simulated results. Fig. 9 shows the comparison between theoretical and simulated results of higher order mode TE_{x21} .

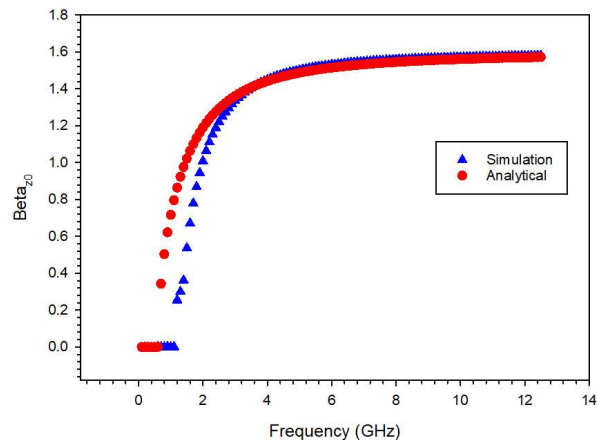


FIGURE 8. Normalized axial phase constant for fundamental mode, TE_{x11} with $\epsilon_r = 2.54$.

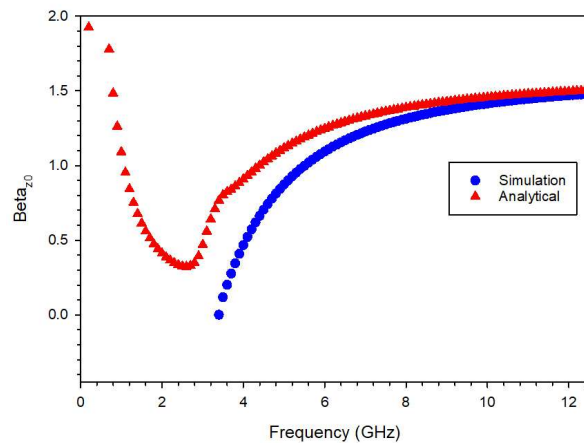


FIGURE 9. Normalized axial phase constant for higher order mode, TE_{x21} with $\epsilon_r = 2.54$.

As shown in Fig. 10, the TE to x fundamental guided mode has E_y and E_z components with $E_x = 0$. Due to the solver's limitations, it cannot be visualized that well in 3D.

4. RADIATION EQUATIONS OF DIELECTRIC HORN ANTENNA

The TE_{10} mode in a hollow metal waveguide excites TE_{x11} hybrid mode as reported in [22] and is also apparent from the

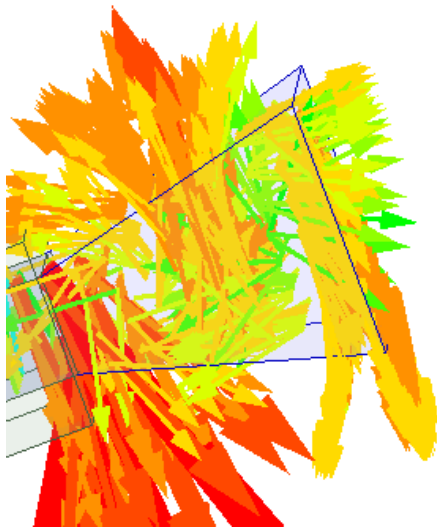


FIGURE 10. TE_{x11} mode in the horn.

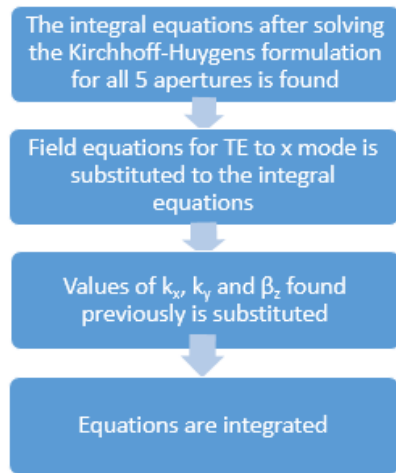


FIGURE 11. Flow chart of steps executed to find the proposed radiation equations.

investigation of the E field pattern of the simulated solid dielectric horn. TE_{x11} hybrid mode has the field component E_x as 0. This hybrid mode is used in Kirchhoff-Huygens formulation [20] for radiation analysis. Since the horn is dielectric, the radiated fields from all five apertures (Fig. 3) have to be analyzed. The equation for radiated E -field from all five apertures (GHCD, ABCD, FEHG, BEHC, and AFGD) is given below, and the methodology adopted for deducing these equations is shown in Fig. 11. Here variations in r direction have been omitted as it is far-field, and ϕ has been resolved into two important components $\phi = 0$ (H -plane) and $\phi = 90$ (E -plane). Thus, the equations are shown with θ variation only. The generation of Eqs. (6)–(13) has been explained through the flowchart in Fig. 11 where radiation of all the above-mentioned apertures is calculated using Kirchhoff-Huygen’s formulation, and the Field equations for TE to x mode (TE_{x11}-fundamental mode is considered) are substituted in places of E_x, E_y, E_z, H_x, H_y & H_z . Then the propagation constant (β_z) found for a particular mode (leaky, fundamental guided TE_{x11} (here) or

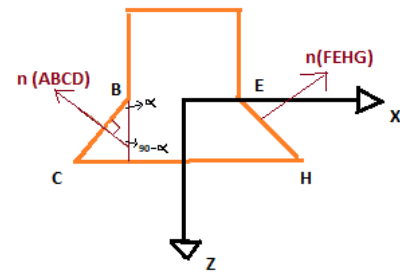


FIGURE 12. Top view of horn.

higher order TE_{xmn}) is substituted, and finally, the equations are integrated using $\phi = 0$ (H -plane) and $\phi = 90$ (E -plane). The TE_{x11} mode is shown in Fig. 10 where $E_x = 0$. The slanted edges, of the horn, are accommodated in the vector n of the Kirchhoff-Huygen formulation, which is implied by looking at geometry as, for example, Fig. 12. Here $n(ABCD) = -\cos \alpha x_0 - \sin \alpha z_0$ and $n(FEHG) = \cos \alpha x_0 - \sin \alpha z_0$.

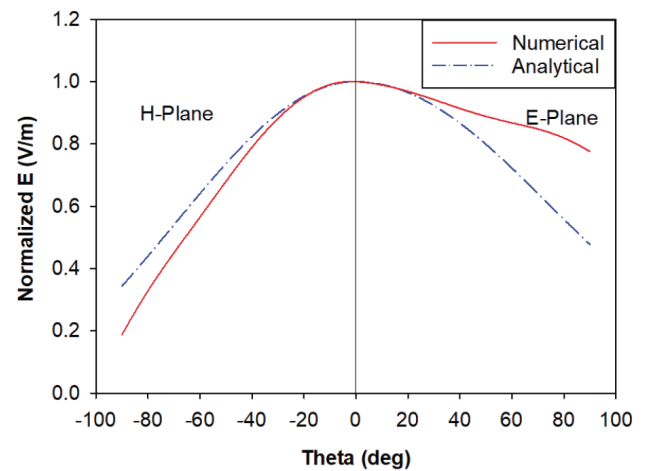


FIGURE 13. E -field pattern at 1.7 GHz (Leaky mode).

H -plane ($\phi = 0^\circ$):

$$E_{pH(GHCD)}(\theta) = -\frac{k_0}{2\pi} \frac{\sin(k_y(\frac{b}{2} + L \tan \xi))}{k_y} \exp(j(k_0 \cos \theta - \beta_z)L) \left(\beta_z \cos \theta + Z_0 \frac{k_1^2 - k_x^2}{\omega \mu_0} \right) M_1 \quad (6)$$

$$E_{pH(ABCD+FEHG)}(\theta) = \frac{j k_0}{4\pi} \left(\cos \alpha \sin \theta \frac{j \beta_z}{k_y} \left(M_2 \cdot \exp \left(j k_0 \sin \theta \frac{a}{2} \right) - M_2' \cdot \exp \left(-j k_0 \sin \theta \frac{a}{2} \right) \right) - \sin \alpha \cos \theta \frac{j \beta_z}{k_y} \left(M_2 \cdot \exp \left(j k_0 \sin \theta \frac{a}{2} \right) + M_2' \cdot \exp \left(-j k_0 \sin \theta \frac{a}{2} \right) \right) \right)$$

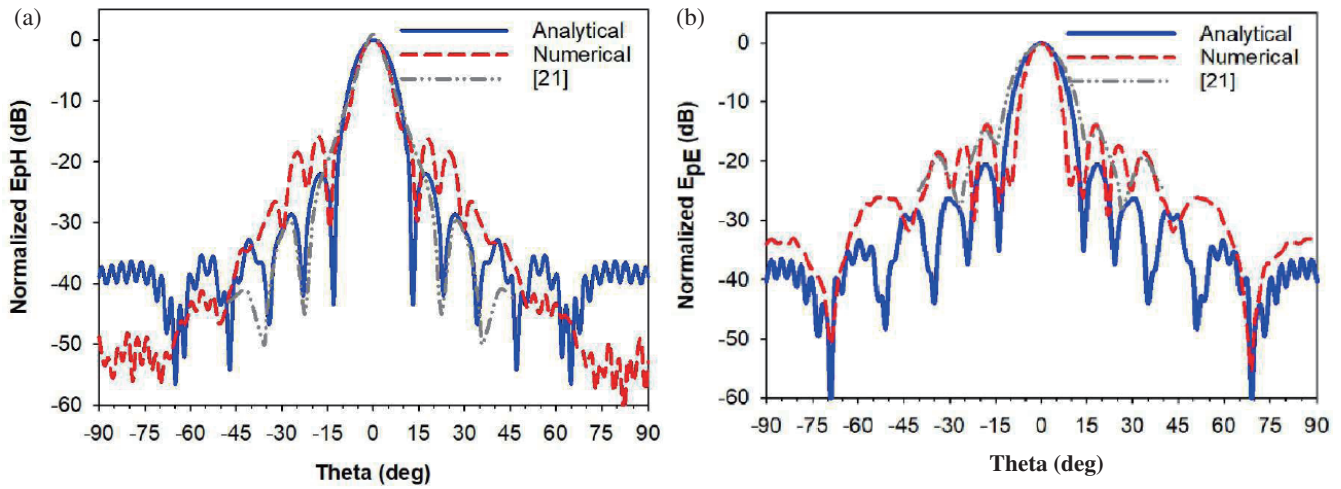


FIGURE 14. Comparison of *E*-field pattern of antenna structure in [21] to proposed theory and simulated result.

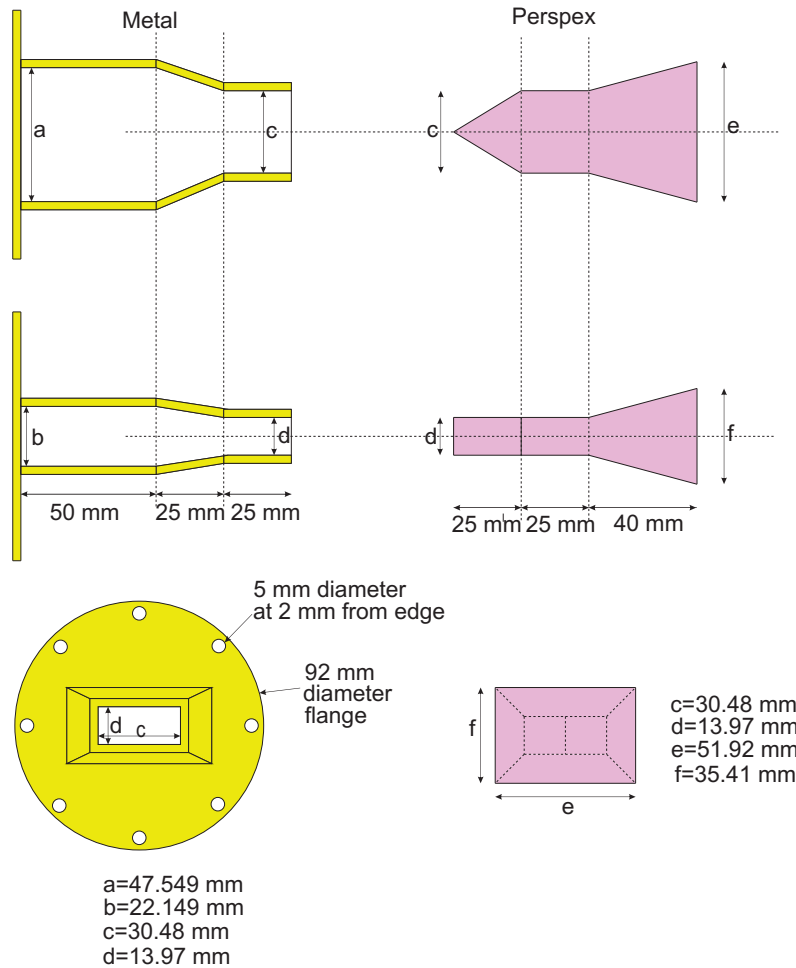


FIGURE 15. Fabricated antenna dimensions.

$$\begin{aligned}
 &+ Z_0 \sin \alpha \frac{k_1^2 - k_x^2}{jk_y \omega \mu_0} \left(M_2 \cdot \exp \left(jk_0 \sin \theta \frac{a}{2} \right) \right. \\
 &+ M'_2 \cdot \exp \left(-jk_0 \sin \theta \frac{a}{2} \right) \left. \right) \\
 &+ Z_0 \cos \alpha \frac{k_x \beta_z}{k_y \omega \mu_0} \left(M_3 \cdot \exp \left(jk_0 \sin \theta \frac{a}{2} \right) \right. \\
 &+ M'_3 \cdot \exp \left(-jk_0 \sin \theta \frac{a}{2} \right) \left. \right) \quad (7)
 \end{aligned}$$

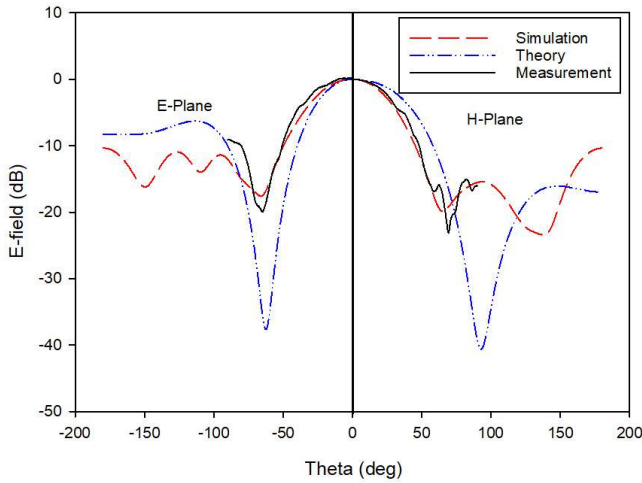


FIGURE 16. Normalized radiated E -field pattern for $\phi = 90^\circ$ (E -Plane) on the left side and $\phi = 0^\circ$ (H -Plane) on the right side at 5 GHz.



FIGURE 18. Fabricated antenna with tapered transition as in [15].

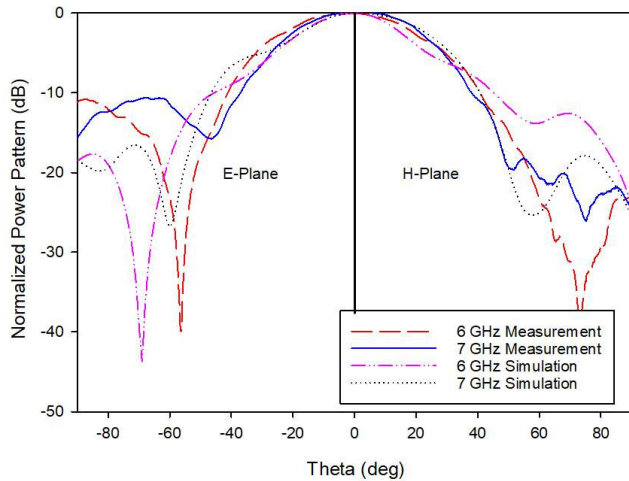


FIGURE 17. Normalized radiated E -field pattern for $\phi = 90^\circ$ (E -Plane) on the left side and $\phi = 0^\circ$ (H -Plane) on the right side at 6 and 7 GHz.

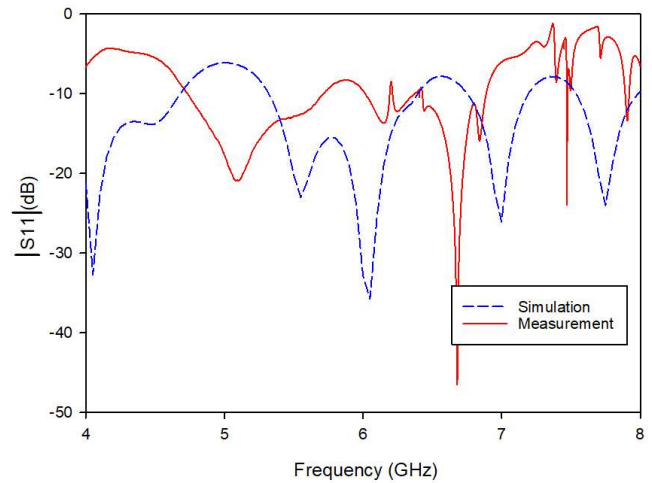


FIGURE 19. Return loss of fabricated antenna.

$$E_{pH(BEHC+AFGD)}(\theta) = \frac{k_0}{2\pi} \left(\sin \xi \cos \theta \beta_z M_6 + j \cos \theta \cos \xi k_y M_9 + Z_0 \sin \xi \frac{k_1^2 - k_x^2}{\omega \mu_0} M_6 \right) \quad (8)$$

E -plane ($\phi = 90^\circ$):

$$E_{pE(GHCD)}(\theta) = -\frac{k_0}{2\pi} \frac{\sin(k_x(\frac{a}{2} + L \tan \alpha))}{k_x} \exp(j(k_0 \cos \theta - \beta_z)L) \left(\beta_z M_{10} + Z_0 \cos \theta \frac{k_1^2 - k_x^2}{\omega \mu_0} M_{10} \right) \quad (9)$$

$$E_{pE(BEHC+AFGD)}(\theta) = \frac{jk_0}{4\pi} \left(-\frac{j\beta_z}{k_x} \sin \xi \left(M_{11} \exp\left(jk_0 \sin \theta \frac{b}{2}\right) \right) \right)$$

$$\begin{aligned} &+ M'_{11} \exp\left(-jk_0 \sin \theta \frac{b}{2}\right) + \frac{k_y}{k_x} \cos \xi \left(M_{12} \exp\left(jk_0 \sin \theta \frac{b}{2}\right) \right) \\ &+ M'_{12} \exp\left(-jk_0 \sin \theta \frac{b}{2}\right) + Z_0 \frac{k_1^2 - k_x^2}{jk_x \omega \mu_0} \cos \xi \sin \theta \\ &\left(M'_{11} \exp\left(-jk_0 \sin \theta \frac{b}{2}\right) - M_{11} \exp\left(jk_0 \sin \theta \frac{b}{2}\right) \right) \\ &+ Z_0 \frac{k_1^2 - k_x^2}{jk_x \omega \mu_0} \sin \xi \cos \theta \left(M_{11} \exp\left(jk_0 \sin \theta \frac{b}{2}\right) \right) \\ &+ M'_{11} \exp\left(-jk_0 \sin \theta \frac{b}{2}\right) \end{aligned} \quad (10)$$

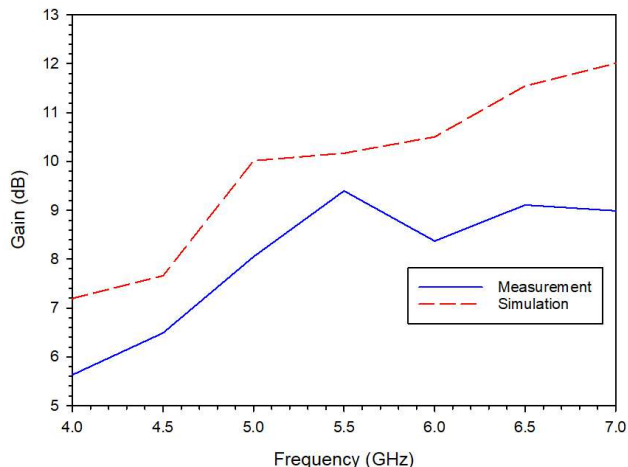


FIGURE 20. Realized gain of fabricated antenna.

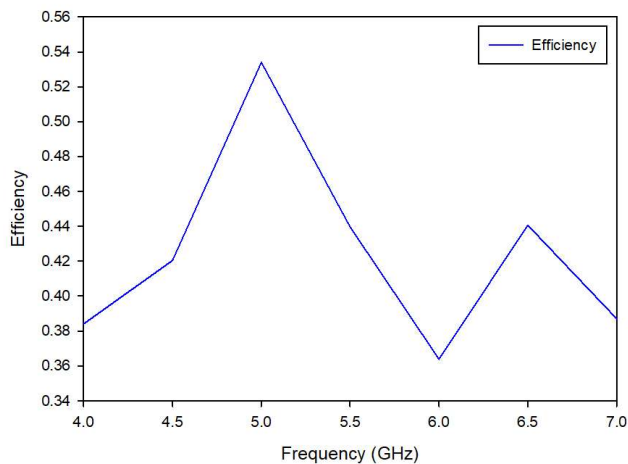


FIGURE 21. Efficiency of the fabricated antenna.

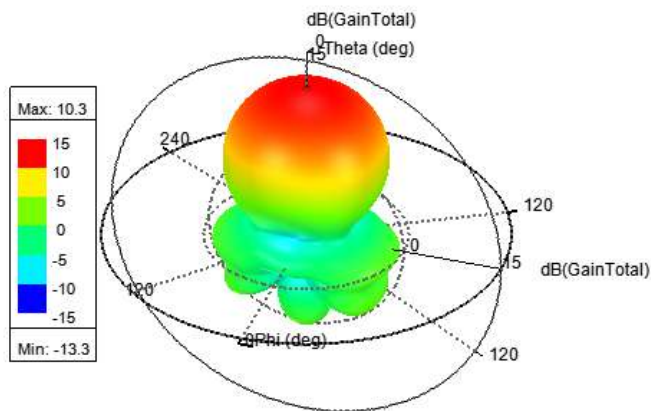


FIGURE 22. 3D plot of radiation pattern at 5 GHz.

$$= \frac{k_0}{2\pi} \left(\beta_z \sin \alpha M_{15} + Z_0 \sin \alpha \cos \theta \frac{k_1^2 - k_x^2}{\omega \mu_0} M_{15} + Z_0 \cos \alpha \sin \theta \frac{k_x k_y}{\omega \mu_0} M_{16} + j Z_0 \cos \alpha \cos \theta \frac{k_x \beta_z}{\omega \mu_0} M_{17} \right) \quad (11)$$

where $M_1, M_2, M'_2, M_3, M'_3, M_6, M_9, M_{10}, M_{11}, M'_{11}, M_{12}, M'_{12}, M_{15}, M_{16}$, and M_{17} are given in Appendix A; Z_0 is the characteristics impedance in the free space; L is the axial length; θ is the angle being considered.

The total E -field is given by:

H -plane ($\phi = 0^\circ$):

$$E_{pH}(\theta) = E_{pH(GHCD)}(\theta) + E_{pH(ABCD+FEHG)}(\theta) + E_{pH(BEHC+AFGD)}(\theta) \quad (12)$$

E -plane ($\phi = 90^\circ$):

$$E_{pE}(\theta) = E_{pE(GHCD)}(\theta) + E_{pE(ABCD+FEHG)}(\theta) + E_{pE(BEHC+AFGD)}(\theta) \quad (13)$$

Equations (6) to (13) are the final reduced form of equations, and they need Appendix A for reference to various variables. Using these equations E -field pattern for a solid dielectric pyramidal horn made of Plexiglass ($\epsilon_r = 3.4$) was found and compared with simulated results in [26] as shown in Fig. 13 and Fig. 14 where the final equations were not included for brevity. Fig. 13 shows leaky mode E -field pattern at 1.7 GHz. In Fig. 14, ‘Analytical’ is the result from the proposed theory applied to the structure in [21]; ‘Numerical’ is the simulation result after the structure in [21] was simulated, and ‘[21]’ is the result presented in [21]. They show a good match which further verifies the equations presented.

5. MEASUREMENT RESULTS

Since Plexiglass with $\epsilon_r = 3.4$ was not readily available in the locality, perspex with a dielectric constant of 2.54 is used for testing the proposed theory as shown in Fig. 15. Using the previously mentioned equations, the normalized E -field pattern at 5 GHz has been presented and set side by side with simulation and measurement results as shown in Fig. 16 where the left side is E -plane results, and the right side is H -plane results. The roots, found from Marcattili’s method [30], are inserted into the radiation equations proposed here as mentioned in Fig. 11. It is observed in Fig. 16 that even though the sidelobe level is not that accurate, the predicted pattern is quite accurate. The formulated results agree fairly with the simulated and measured results, which validate the proposed radiation equations. The simulated and measured radiation patterns are plotted in Fig. 17 for the fabricated structure at 6 and 7 GHz.

The fabricated antenna with a dielectric constant of 2.54 is shown in Fig. 18. The measured return loss is shown in Fig. 19, and WR187 waveguide adapter was used to excite the horn, which worked from 3.95 GHz to 5.85 GHz. The simulated results did not include WR187 waveguide to coax adapter. The fabricated antenna was measured in the Space Applications Centre, Indian Space Research Organization test facility. The plot shows that the antenna operates from 4.7 GHz to 6.9 GHz.

$$E_{pE(ABCD+FEHG)}(\theta)$$

The realized gain of the fabricated antenna was measured and is shown in Fig. 20. The simulated gain was generated just with the horn antenna and transition without the WR187 waveguide to coax adapter. Thus, there is a significant difference between the measured and simulated gains. Fig. 21 shows the measured efficiency of the antenna. Fig. 22 shows the 3D plot of the radiation pattern at 5 GHz.

The novel transition presented by the authors in [15] works well with $\epsilon_r = 2.54$, which is expected as only above this range of dielectric constant selection there is a higher probability of generating higher modes [20]. Here, we have selected easily available Perspex material for manufacturing. We will continue our experimentation depending on the availability of Plexiglass of dielectric constant 3.4.

6. CONCLUSION

In plasma diagnostics and integrated circuits, solid dielectric horn antenna is preferred since it gives higher gain than a metal horn and without the fabrication complexity. Thus, a comprehensive study of propagation and radiation characteristics of solid dielectric horn antenna becomes pertinent.

Here, we propose a theory for propagation and radiation characteristics for leaky mode in a solid dielectric horn antenna. This theory can be applied to fundamental guided and higher-order guided modes as well. The results of equations for propagation characteristics for guided and leaky modes of solid dielectric horn antenna are validated by the simulation results. Further, the proposed E -field equations, omitted earlier in [26], fairly predict the radiated fields for guided mode and leaky antenna mode, which is corroborated further by the comparison with measured results. Thus, the theory of radiation proposed can give the designer a better insight and enhance the interpretation of the simulation results like analyzing if the pattern is due to just the fundamental mode or higher-order guided modes or leaky modes. From the plotted graphs given in this paper, we can infer equations for propagation characteristics and predict the dispersion relations well. Also, the proposed radiation equations predict the radiation pattern of guided and leaky modes well.

The solid dielectric horn antenna presented will also be fabricated in Plexiglass in the future, and measurement results will be compared to analytical and numerical results in [26].

ACKNOWLEDGEMENT

The authors thank CSIR Emeritus Scientist Scheme for financially supporting this research. We also acknowledge Dr. C. K. Aanandan, ACARR, CUSAT, Cochin, India, and Dr. Deepti Das Krishna for their mentorship during the CSIR Emeritus Scientist Scheme. The authors also thank K. K. Sood and Jigar Pandya from SAC-ISRO for providing antenna measurement facilities.

APPENDIX A. VARIABLES USED IN THE PAPER

$M_1, M_2, M'_2, M_3, M'_3, M_6, M_9, M_{10}, M_{11}, M'_{11}, M_{12}, M'_{12}, M_{15}, M_{16}$ and M_{17} are the variables used in Eqs. (6) to (11)

and are given in this Appendix.

$$M_1 = \frac{\sin\left((k_0 \sin \theta + k_x)\left(\frac{a}{2} + L \tan \alpha\right)\right)}{k_0 \sin \theta + k_x} + \frac{\sin\left((k_0 \sin \theta - k_x)\left(\frac{a}{2} + L \tan \alpha\right)\right)}{k_0 \sin \theta - k_x} \quad (\text{A1})$$

$$M_2 = N_{\alpha 11}^0 - N_{\alpha 12}^0 \quad (\text{A2})$$

$$M_3 = N_{\alpha 21}^0 - N_{\alpha 22}^0 \quad (\text{A3})$$

$$M'_2 = N_{\alpha 11}^1 - N_{\alpha 12}^1 \quad (\text{A4})$$

$$M'_3 = N_{\alpha 21}^1 - N_{\alpha 22}^1 \quad (\text{A5})$$

$$M_6 = \frac{1}{2} \left(\frac{L_{122} + L_{121}}{(k_0 \sin \theta + k_x)} + \frac{L_{112} + L_{111}}{(k_0 \sin \theta - k_x)} \right) \quad (\text{A6})$$

$$M_9 = \frac{1}{2} \left(\frac{L_{221} - L_{222}}{(k_0 \sin \theta + k_x)} + \frac{L_{211} + L_{212}}{(k_0 \sin \theta - k_x)} \right) \quad (\text{A7})$$

$$M_{10} = \frac{\sin\left((k_0 \sin \theta + k_y)\left(\frac{b}{2} + L \tan \xi\right)\right)}{(k_0 \sin \theta + k_y)} + \frac{\sin\left((k_0 \sin \theta - k_y)\left(\frac{b}{2} + L \tan \xi\right)\right)}{(k_0 \sin \theta - k_y)} \quad (\text{A8})$$

$$M_{11} = N_{\xi 11}^0 + N_{\xi 12}^0 \quad (\text{A9})$$

$$M_{12} = N_{\xi 21}^0 - N_{\xi 22}^0 \quad (\text{A10})$$

$$M'_{11} = N_{\xi 11}^1 + N_{\xi 12}^1 \quad (\text{A11})$$

$$M'_{12} = N_{\xi 21}^1 - N_{\xi 22}^1 \quad (\text{A12})$$

$$M_{15} = \frac{1}{2} \left(\frac{K_{122} + K_{112}}{(k_0 \sin \theta + k_y)} + \frac{K_{121} + K_{111}}{(k_0 \sin \theta - k_y)} \right) \quad (\text{A13})$$

$$M_{16} = \frac{j}{2} \left(\frac{K_{222} - K_{212}}{(k_0 \sin \theta + k_y)} + \frac{K_{211} - K_{221}}{(k_0 \sin \theta - k_y)} \right) \quad (\text{A14})$$

$$M_{17} = \frac{1}{2} \left(\frac{K_{212} - K_{222}}{(k_0 \sin \theta + k_y)} + \frac{K_{211} - K_{221}}{(k_0 \sin \theta - k_y)} \right) \quad (\text{A15})$$

$$N_{\tau np}^q = \left((k_0 \cos \theta + (-1)^q k_0 \sin \theta \tan \tau - \beta_z) \right) \left((k_0 \cos \theta + (-1)^q k_0 \sin \theta \tan \tau - \beta_z)^2 - (k_x \tan \alpha + (-1)^{n+p} k_y \tan \xi)^2 \right)^{-1} \left(-j \left(\sin \left((n-1) \frac{\pi}{2} + \left(k_x \left(\frac{a}{2} + z_1 \tan \alpha \right) + (-1)^{n+p} k_y \left(\frac{b}{2} + z_1 \tan \xi \right) \right) \right) \right) \exp \left(j(k_0 \cos \theta \right.$$

$$\begin{aligned}
 & +(-1)^q k_0 \sin \theta \tan \tau - \beta_z) z_1) - \sin((n-1) \frac{\pi}{2} \\
 & + \left(k_x \frac{a}{2} + (-1)^{n+p} k_y \frac{b}{2} \right) \Big) \Big) \\
 & + \frac{(k_x \tan \alpha + (-1)^{n+p} k_y \tan \xi)}{(k_0 \cos \theta + (-1)^q k_0 \sin \theta \tan \tau - \beta_z)} \\
 & \left(\cos \left((n-1) \frac{\pi}{2} - \left(k_x \left(\frac{a}{2} + z_1 \tan \alpha \right) + (-1)^{n+p} k_y \right. \right. \right. \\
 & \left. \left. \left. \left(\frac{b}{2} + z_1 \tan \xi \right) \right) \right) \right) \exp(j(k_0 \cos \theta + (-1)^q k_0 \sin \theta \tan \tau - \beta_z) z_1) \\
 & - \cos \left((n-1) \frac{\pi}{2} - \left(k_x \frac{a}{2} + (-1)^{n+p} k_y \frac{b}{2} \right) \right) \Big) \Big) \quad (A16)
 \end{aligned}$$

$$\begin{aligned}
 L_{npq} &= (k_0 \cos \theta - \beta_z) ((k_0 \cos \theta - \beta_z)^2 \\
 & - ((k_0 \sin \theta + (-1)^p k_x) \tan \alpha + (-1)^q k_y \tan \xi)^2)^{-1} \\
 & \left(-j \left(\sin \left((n-1) \frac{\pi}{2} + \left((k_0 \sin \theta + (-1)^p k_x \right) \right. \right. \right. \\
 & \left. \left. \left. \left(\frac{a}{2} + z_2 \tan \alpha \right) + (-1)^q k_y \left(\frac{b}{2} + z_2 \tan \xi \right) \right) \right) \right) \\
 & \exp(j(k_0 \cos \theta - \beta_z) z_2) - \sin \left((n-1) \frac{\pi}{2} \right. \\
 & \left. + \left((k_0 \sin \theta + (-1)^p k_x) \frac{a}{2} + (-1)^q k_y \frac{b}{2} \right) \right) \Big) \Big) \\
 & + \frac{(k_0 \sin \theta + (-1)^p k_x) \tan \alpha + (-1)^q k_y \tan \xi}{k_0 \cos \theta - \beta_z} \\
 & \left(\cos \left((n-1) \frac{\pi}{2} - \left((k_0 \sin \theta + (-1)^p k_x \right) \right. \right. \right. \\
 & \left. \left. \left. \left(\frac{a}{2} + z_2 \tan \alpha \right) + (-1)^q k_y \left(\frac{b}{2} + z_2 \tan \xi \right) \right) \right) \right) \\
 & \exp(j(k_0 \cos \theta - \beta_z) z_2) - \cos \left((n-1) \frac{\pi}{2} \right. \\
 & \left. - \left((k_0 \sin \theta + (-1)^p k_x) \frac{a}{2} + (-1)^q k_y \frac{b}{2} \right) \right) \Big) \Big) \quad (A17)
 \end{aligned}$$

$$\begin{aligned}
 K_{npq} &= ((k_0 \cos \theta - \beta_z) ((k_0 \cos \theta - \beta_z)^2 \\
 & - ((k_0 \sin \theta + (-1)^q k_y) \tan \xi + (-1)^p k_x \tan \alpha)^2)^{-1} \\
 & \left(-j \left(\sin \left((n-1) \frac{\pi}{2} + \left((k_0 \sin \theta + (-1)^q k_y \right) \right. \right. \right.
 \end{aligned}$$

$$\begin{aligned}
 & \left(\frac{b}{2} + z_1 \tan \xi \right) + (-1)^p k_x \left(\frac{a}{2} + z_1 \tan \alpha \right) \Big) \Big) \\
 & \exp(j(k_0 \cos \theta - \beta_z) z_1) - \sin \left((n-1) \frac{\pi}{2} \right. \\
 & \left. + \left((k_0 \sin \theta + (-1)^q k_y) \frac{b}{2} + (-1)^p k_x \frac{a}{2} \right) \right) \\
 & - \frac{((k_0 \sin \theta + (-1)^q k_y) \tan \xi + (-1)^p k_x \tan \alpha)}{(k_0 \cos \theta - \beta_z)} \\
 & \left(\cos \left((n-1) \frac{\pi}{2} - \left((k_0 \sin \theta + (-1)^q k_y \right) \right. \right. \right. \\
 & \left. \left. \left. \left(\frac{b}{2} + z_1 \tan \xi \right) + (-1)^p k_x \left(\frac{a}{2} + z_1 \tan \alpha \right) \right) \right) \right) \\
 & \exp(j(k_0 \cos \theta - \beta_z) z_1) - \cos \left((n-1) \frac{\pi}{2} \right. \\
 & \left. - \left((k_0 \sin \theta + (-1)^q k_y) \frac{b}{2} + (-1)^p k_x \frac{a}{2} \right) \right) \Big) \Big) \quad (A18)
 \end{aligned}$$

REFERENCES

- [1] Chatterjee, R., "Dielectric and dielectric-loaded antennas," *NASA STI/Recon Technical Report A*, Vol. 86, 1985.
- [2] Bartlett, H. and R. Moseley, "Dielectric waveguides — Novel, highly efficient, low noise antenna feed systems," *1965 Antennas and Propagation Society International Symposium*, Washington, DC, USA, 217–225, 1965.
- [3] Wang, L., M. Garcia-Vigueras, M. Alvarez-Folgueiras, and J. R. Mosig, "Wideband *H*-plane dielectric horn antenna," *IET Microwaves, Antennas & Propagation*, Vol. 11, No. 12, 1695–1701, 2017.
- [4] Friedrich, A., B. Geck, and M. Fengler, "LDS manufacturing technology for next generation radio frequency applications," *2016 12th International Congress Molded Interconnect Devices (MID)*, *IEEE*, 1–6, Sep. 2016.
- [5] Friedrich, A., B. Geck, and M. Fengler, and A. Fischer, "24 GHz dielectric filled waveguide fed horn antenna using 3D-LDS MID technology," *2016 46th European Microwave Conference (EuMC)*, *IEEE*, 739–742, Oct. 2016.
- [6] Friedrich, A., M. Fengler, B. Geck, and D. Manteuffel, "60 GHz 3D integrated waveguide fed antennas using laser direct structuring technology," *2017 11th European Conference on Antennas and Propagation (EUCAP)*, *IEEE*, 2507–2510, Mar. 2017.
- [7] Pousi, J. P., D. V. Lioubtchenko, S. Dudorov, and A. V. Raisanen, "High permittivity dielectric rod waveguide as an antenna array element for millimeter waves," *IEEE Transactions on Antennas and Propagation*, Vol. 58, No. 3, 714–719, Mar. 2010.
- [8] Cambor, R., S. V. Hoeye, C. Vázquez, G. Hotopan, M. Fernández, A. Hadarig, and F. Las-Heras, "Submillimeter wave 8×1 antenna array with dielectric rods to improve the radiation pattern," *2013 European Radar Conference*, 375–378, 2013.
- [9] Nguyen, T. P., C. Pichot, C. Migliaccio, and W. Menzel, "Study of folded reflector multibeam antenna with dielectric rods as primary source," *IEEE Antennas and Wireless Propagation Letters*, Vol. 8, 786–789, 2009.
- [10] Rivera-Lavado, A., et al., "Dielectric rod waveguide antenna as THz emitter for photomixing devices," *IEEE Transactions on Antennas and Propagation*, Vol. 63, No. 3, 882–890, Mar. 2015.

- [11] Kobayashi, S., R. Mittra, and R. Lampe, "Dielectric tapered rod antennas for millimeter-wave applications," *IEEE Transactions on Antennas and Propagation*, Vol. 30, No. 1, 54–58, 1982.
- [12] Shiau, Y., "Dielectric rod antennas for millimeter-wave integrated circuits (short papers)," *IEEE Transactions on Microwave Theory and Techniques*, Vol. 24, No. 11, 869–872, Nov. 1976.
- [13] Dudorov, S., "Rectangular dielectric waveguide and its optimal transition to a metal waveguide," Ph.D. Thesis, 2002.
- [14] Wang, L., Garcia-Vigueras, M. Alvarez-Fogueiras, M. Mosig, and R. Juan, "Wideband H -plane dielectric horn antenna," *IET Microwaves, Antennas & Propagation*, Vol. 11, No. 12, 1695–1701, 2017.
- [15] Menon, S. S., D. D. Krishna, C. K. Aanandan, and S. K. Pathak, "Guided and leaky mode characteristics of solid dielectric horn: Analytical and numerical solutions," *2020 IEEE International Symposium on Antennas and Propagation and North American Radio Science Meeting*, 279–280, 2020.
- [16] Tiwari, V. N., T. Tiwari, S. P. Singh, and R. K. Jha, "Far field patterns of solid dielectric diagonal horn antennas," *International Journal of Electronics*, Vol. 82, No. 2, 175–192, 1997.
- [17] Tiwari, V. N., T. Tiwari, S. P. Singh, and R. K. Jha, "Near field distribution of solid dielectric diagonal horn antennas," *International Journal of Electronics*, Vol. 82, No. 2, 167–174, 1997.
- [18] Jha, B. and R. K. Jha, "Surface fields of the H -plane sectoral dielectric horn antenna," *1985 15th European Microwave Conference*, 433–438, Paris, France, 1985.
- [19] Singh, A. K., B. Jha, and R. K. Jha, "Near-field analysis of E -plane sectoral solid dielectric horn antennas," *International Journal of Electronics*, Vol. 71, No. 4, 697–706, 1991.
- [20] Salema, C., C. Fernandes, and R. K. Jha, *Solid Dielectric Horn Antennas*, Artech House Publishers, 1998.
- [21] Brooking, N., P. J. B. Clarricoats and A. D. Olver, "Radiation patterns of pyramidal dielectric waveguides," *Electronics Letters*, Vol. 10, No. 3, 33–34, Feb. 7, 1974.
- [22] Singh, A. K., R. Chaudhari, B. Jha, and R. K. Jha, "Radiation pattern of E -plane sectoral solid dielectric horn antennas," *International Journal of Electronics*, Vol. 73, No. 1, 203–213, 1992.
- [23] Tiwari, V. N., T. Tiwari, and R. K. Jha, "Comparative studies of near field distributions of solid and hollow dielectric diagonal horn antennas," *Proceedings of the International Conference on Electromagnetic Interference and Compatibility '99 (IEEE Cat. No. 99TH 8487)*, 241–244, Hyderabad, India, 1997.
- [24] Menon, S. S., J. K. Bhalani, and S. K. Pathak, "Propagation characteristics of guided modes in a solid dielectric pyramidal horn," *2012 International Conference on Communication Systems and Network Technologies*, 71–75, Rajkot, 2012.
- [25] Roy, P. S., M. Guha, and M. Asifuzzaman, "Investigations and enhancement of aperture solid dielectric pyramidal and cone horn antenna in X band applications," *International Journal of Electronics Engineering*, Vol. 11, No. 1, 130–135, Jun. 2019.
- [26] Menon, S. S., D. D. Krishna, C. K. Aanandan, and S. K. Pathak, "Guided and leaky mode radiation characteristics of solid dielectric pyramidal horn," *2021 IEEE International Symposium on Antennas and Propagation and North American Radio Science Meeting*, 2021.
- [27] Menon, S. and S. Pathak, *Guided Modes in Solid Dielectric Horn Antenna: Propagation Characteristics of Guided Modes in Solid Dielectric Horn Antenna*, LAP LAMBERT Academic Publishing, Jul. 24, 2012.
- [28] Hu, J. and C. R. Menyuk, "Understanding leaky modes: slab waveguide revisited," *Advances in Optics and Photonics*, Vol. 1, No. 1, 58–106, 2009.
- [29] Ishimaru, A., *Electromagnetic Wave Propagation, Radiation, and Scattering from Fundamentals to Applications*, IEEE Press Wiley, 2017.
- [30] Marcattili, E. A. J., "Dielectric rectangular waveguide and directional coupler for integrated optics," *Bell System Technical Journal*, Vol. 48, 2017–2102, 1969.
- [31] Yeh, C. and F. I. Shimabukuro, *The Essence of Dielectric Waveguides*, Springer, New York, 2008.
- [32] Balanis, C. A., *Advanced Engineering Electromagnetics*, John Wiley & Sons, 1999.
- [33] Lampariello, P., F. Frezza, H. Shigesawa, M. Tsuji, and A. A. Oliner, "A versatile leaky-wave antenna based on stub-loaded rectangular waveguide, I. Theory," *IEEE Transactions on Antennas and Propagation*, Vol. 46, No. 7, 1032–1041, Jul. 1998.